6.3 RAPID SAMPLING OF RADAR PRECURSOR SIGNATURES ASSOCIATED WITH MULTIPLE DOWNBURSTS ON 14 JUNE 2011

Charles M. Kuster*[1,3], Pamela L. Heinselman[2,3], and Terry J. Schuur[1,3]

[1]Cooperative Institute for Mesoscale Meteorological Studies, [2]NOAA/OAR National Severe Storms Laboratory, [3]University of Oklahoma, Norman, Oklahoma

1. INTRODUCTION

Over the past several decades, downburst studies have frequented the literature primarily due to the hazards they present to aircraft. Fujita and collaborators pioneered research of this phenomenon after the crash of an airliner at John F. Kennedy Airport in 1975. Fujita and Byers (1977) identified the event as a downburst and defined it as a particularly intense downdraft with vertical motions higher than about 3.5 m s^{-1}. Later work addressed the spatial coverage of downbursts by classifying damaging winds with horizontal diameters less than 4 km as microbursts and those with horizontal diameters greater than 4 km as macrobursts (Fujita and Wakimoto 1981; Wakimoto 2001). Through aerial surveys (Fujita 1981) he also recognized the potential risks to man-made structures posed by winds potentially exceeding 50 m s^{-1}.

With a definition in place, numerical simulations and environmental observations focused on determining the conditions favorable for the development of downbursts. Modeling studies (e.g., Srivastava 1987; Proctor 1988; Straka and Anderson 1993) have shown the importance of the melting of ice-phase hydrometeors in increasing negative buoyancy, thereby leading to a stronger downdraft. Other factors, such as precipitation loading, also appeared to play a role in the development and intensity of a downdraft, but the two most important drivers were the melting and evaporation of precipitation (Proctor 1988). Observations of environmental soundings suggested that steep lapse rates, high melting layers, and relatively high low-level relative humidities can signal an enhanced potential for damaging downbursts (Srivastava 1985; Proctor 1988).

Advancements in weather radar technology also increased understanding and predictability of downbursts by allowing meteorologists to observe precursor signatures associated with these events. Roberts and Wilson (1989) studied 31 storms in Colorado and noted the existence of enhanced midlevel radial convergence several minutes prior to the detection of a divergent signature at the surface. This observation was supported by calculations using the mass continuity equation, which showed that air would converge inward in response to a rapidly descending downdraft. They also observed an area of heightened reflectivity values that developed approximately 5–8 km above the surface before rapidly descending only minutes prior to a downburst. This feature became known as the descending reflectivity core (DRC). Further research has confirmed the existence of these precursor signatures in Alabama (Isaminger 1988), Oklahoma (Eilts 1987), and Arizona (Vasiloff and Howard 2009).

The advent of dual-polarization radar technology (e.g., Balakrishnan and Zrnić 1990; Doviak and Zrnić 1993; Zrnić and Rhyzhkov 1999) further increased downburst knowledge by revealing information about microphysical processes within thunderstorms. Proctor (1988) demonstrated the importance of melting in downdraft intensity, thereby making a precursor signature indicative of melting helpful in predicting downbursts. This precursor signature, known as a Z_{DR} hole, consists of a narrow region of near-zero differential reflectivity (Z_{DR}) completely surrounded by positive values of Z_{DR}, all below the environmental melting layer (Wakimoto and Bringi 1988; Roberts and Wilson 1989). This signature suggests the presence of hail below the melting layer, which must at least partially melt.

Recent work has focused on new technology to better observe downbursts. The National Weather Radar Testbed Phased-Array Radar (NWRT PAR, hereafter PAR), located in Norman, Oklahoma, uses electronic beam steering to complete traditional volume scans, such as volume coverage pattern (VCP) 12 (Brown et al. 2005), in approximately one minute (Heinselman et al. 2008). With this enhanced temporal resolution, meteorological features, such as downburst precursor signatures, can be better resolved, effectively augmenting detectability and predictability. Heinselman et al. (2008) showed the minute-by-minute evolution of midlevel convergence and a DRC associated with a downburst in Oklahoma. Over the 18-minute life cycle of the precursor signatures, the PAR collected 16 volume scans. A traditional radar using VCP 12 would have only completed about 4 volume scans during the same period. Therefore, a more accurate picture of the evolution and trends of precursor signatures can be obtained with the PAR.

The purpose of this study is to employ rapid-sampling capabilities of the PAR to analyze radar precursor signatures associated with a unique thunderstorm that produced a series of downbursts in central Oklahoma. This storm was ideal for rapid sampling for several reasons. It was relatively intense (inferred from the widespread reflectivity values over 65 dBZ), rapidly evolved into a multicell thunderstorm that produced multiple severe and non-severe downbursts, and exhibited storm-scale features that evolved rather rapidly. For example, high-reflectivity cores developed and descended to near the surface in as little as 11 minutes, while some near-surface divergent signatures persisted for less than 10 minutes. Changes on this time scale require much higher temporal resolution than that provided by conventional radars in order to more fully understand and observe the trends in precursor signatures.

This paper focuses on one severe and one non-severe downburst produced on 14 June 2011. For this study, a

* *Corresponding author address:* Charles Kuster, University of Oklahoma, 120 David L. Boren Blvd., Norman, OK, 73073; e-mail: charles.kuster@noaa.gov

downburst is classified as severe if a damaging wind report existed for the event, or if the near-surface Doppler velocities reached 25.7 m s^{-1} (50 knots) or higher. All other downbursts are classified as non-severe. For each downburst, an in-depth analysis of the DRC and midlevel radial convergence is presented. Associated dual-polarization radar precursor signatures are also analyzed, though in much less detail due to the coarse temporal resolution of the available data.

2. RADAR DATA

The PAR and a dual-polarization Weather Surveillance Radar 1988-Doppler (WSR-88D) research radar (KOUN) provided data for analysis. These radars are nearly co-located (approximately 120 m apart) in Norman, Oklahoma and have wavelengths near 10 cm (S-band). Both radars operated during the entire analysis period, which stretches from 2330-0021 UTC. The PAR employed a modified VCP 12 (Brown et al. 2005), containing an additional five elevation angles above 19.50º. An algorithm called ADAPTS (Heinselman and Torres 2011) was used to further decrease volume-scan update times by only scanning locations containing, or adjacent to, weather-related echoes. This technique provided volume-scan update times of 50 s during the beginning of the event and 63 s by the end of the data analysis window. KOUN utilized VCP 11 (Brown and Wood 2000) with an update time of about five minutes.

3. EVENT BACKGROUND

The Norman, Oklahoma 0000 UTC 15 June 2011 sounding (Fig. 1) revealed thermodynamic conditions conducive for downbursts. A deep well-mixed boundary layer stretched upwards from the surface to approximately 3.2 km above mean sea level (MSL). Dew point depressions in this layer ranged from 20 ºC at the surface to 4 ºC near 3.2 km MSL, giving the low-levels of the sounding an "inverted V" appearance. Instability was modest with CAPE values around 1500 J kg^{-1}. The storm of interest initially developed at about 2239 UTC just south of a surface cold front draped across central Oklahoma. Within 1.5 hours, the storm had developed into a large multicellular complex with multiple high-reflectivity cores (Fig. 2). Between 2358–0021 UTC, three severe downbursts and two non-severe downbursts were sampled by the PAR and KOUN. To differentiate between downbursts, a naming scheme was developed which assigned a primary key of "MAB" to severe downbursts and a "Null" to non-severe downbursts. A letter followed each primary key depending on their chronological order. Therefore, the first severe downburst was named MAB-a while the first non-severe downburst was named Null-a (Table 1). The following analysis focuses on MAB-a and Null-b.

4. RADAR DATA ANALYSIS AND RESULTS

To quantify the vertical extent of the DRCs associated with each downburst, vertical cross sections were used to determine the highest and lowest occurrence of the 65 dBZ isosurface. This method was used to track the development and descent of each high-reflectivity core over time. The linear least squares derivatives divergence field (Smith and

Severe		Non-Severe	
Downburst	**Time (UTC)**	**Downburst**	**Time (UTC)**
MAB-a	23:58:13	Null-a	0:00:19
MAB-b	0:06:06	Null-b	0:02:25
MAB-c	0:09:14		
MAB-cd	0:18:01		

Table 1. Names and approximate beginning times of all severe and non-severe downbursts produced during the analysis window.

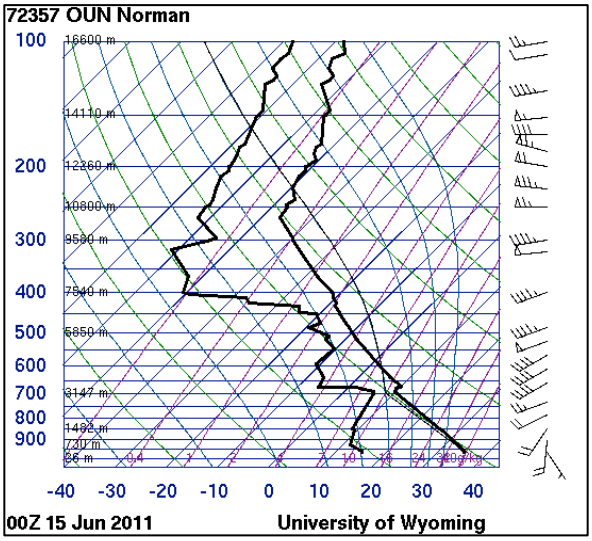

Figure 1. 00Z 15 June 2011 Norman, Oklahoma sounding.

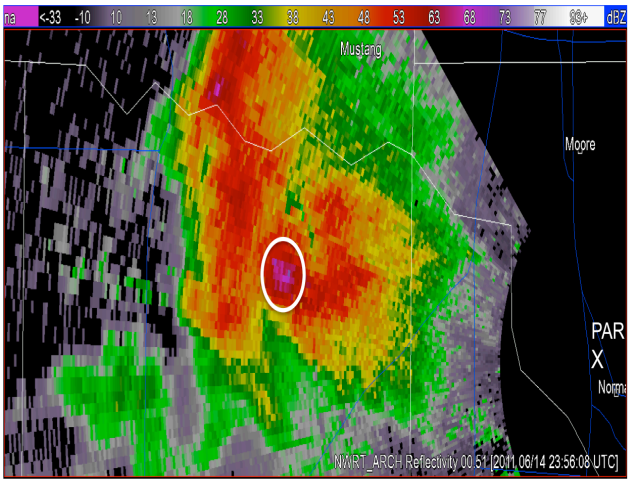

Figure 2. The .51° reflectivity field from 2356 UTC showing the high-reflectivity core associated with MAB-a (white circle).

Elmore 2004) provided a means to measure the magnitude and evolution of the midlevel radial convergence/divergence (hereafter convergence/divergence). Divergence values from this field, corresponding to each high-reflectivity core and the immediately adjacent range gates, were retrieved and then averaged over an analysis depth of 1–7 km above radar level (ARL) to produce a single divergence value for each volume scan.

4.1 MAB-a

The PAR initially sampled the near-surface divergence signature associated with this severe downburst at 2358 UTC (hereafter all times are in UTC). Four minutes later, the PAR sampled a maximum base velocity of 22.5 m s^{-1} (44 knots), which served as the time of maximum downburst intensity. At 2305, the downburst produced a severe wind gust of 29 m s^{-1} (56 knots), which caused minor tree damage near Tuttle, Oklahoma (NWS Performance Management 2011) before dissipating by 0008. Approximately 22 minutes prior to the maximum sampled base velocity, the high-reflectivity core associated with MAB-a was first sampled. From this time, the bottom of the core slowly descended until 2348 (Fig. 3). Its height remained unchanged for roughly two minutes, before descending to near the surface by 2355. The height of the top of the core remained essentially static during the early portions of DRC evolution before beginning to descend around 2349. There was a brief pause in descent, similar to that observed with the bottom of the core, between 2353–2354, before continuous and more rapid descent commenced about eight minutes prior to the maximum intensity of the downburst. The top and bottom of the high-reflectivity core followed a similar pattern of descent, but there was a lag time of several minutes between the two. For example, continuous and more rapid descent of the bottom of the core began approximately 4 minutes prior to continuous descent of the top of the core.

A distinct pattern emerged when analyzing the magnitude of the midlevel convergence with this event (Fig 4). The convergence magnitude increased with time before reaching a maximum value of -.0006 s^{-1} at 2354. After this time, the convergence magnitude decreased for the duration of the signature's existence. This evolution follows the laws of mass continuity. As the downdraft descended through the depth of the analysis height (1–7 km ARL), the convergence reached a peak in intensity, that occurred near the time of rapid descent in both the top and bottom of the high-reflectivity core (Fig. 5). Then, as the top of the core continued to descend through the analysis height, the overall downdraft depth (inferred by the DRC) decreased, which possibly led to the continuous decrease in midlevel convergence magnitude.

4.2 Null-b

The PAR initially sampled the near-surface divergence signature associated with this non-severe downburst at 0002. No damaging wind reports were received for this downburst and the maximum base velocity of 14.0 m s^{-1} (27 knots) was sampled at 0006. Approximately 13 minutes prior to maximum intensity, the PAR sampled the first instance of the 65 dBZ isosurface, signaling the approximate beginning of the downburst's high-reflectivity core. The bottom of the core slowly and continuously descended through the duration of the DRC signature, reaching near the surface by 0003 (Fig. 6). The top of the core evolved differently than the bottom of the core, in that its height increased with time, reaching a maximum height just over 10 km MSL at 2357. Continuous descent then occurred, but only up to the initial sampling of the near-surface downburst. It is unclear why the top of the core stopped descending at 0002, but perhaps this evolution played a role in limiting the maximum intensity of the downburst.

The evolution of midlevel convergence magnitude associated with this downburst followed a “flat line” pattern, fluctuating only slightly prior to downburst occurrence (Fig. 7). The maximum magnitude of midlevel convergence reached a peak value just above -.0003 s^{-1} at 0002. The pattern and magnitude of convergence remained consistent with the notion of mass continuity. A lack of rapid descent within this portion of the thunderstorm precluded the development of strong convergence. Just prior to the time of maximum downburst intensity, a sharp decrease in midlevel convergence occurred and became divergent on average. The marked decrease in convergence may have resulted from the initial development of a strong mesoscale divergent signature produced by larger scale outflow within the multicell thunderstorm complex.

4.3 Dual-Polarization Precursor Signatures

The primary dual-polarization precursor signature analyzed was the Z_{DR} hole. Tracking and analyzing the evolution of this signature over time proved very challenging due to the coarser temporal resolution of the KOUN data. The data “snap shots” allowed for the identification of precursor signatures for both downbursts, but prevented a more in-depth analysis of the full evolution of the signatures. In this case, a Z_{DR} hole was observed with both the severe and non-severe downbursts. Both Z_{DR} holes were generally co-located with the high-reflectivity cores observed in the PAR data. The Z_{DR} hole associated with MAB-a initially developed at approximately 2344, 18 minutes prior to the maximum downburst intensity. The Z_{DR} hole associated with Null-b initially developed at approximately 2359, 5 minutes prior to the maximum downburst intensity. The presence of the Z_{DR} hole indicated melting hail, but did not help differentiate downdraft intensity.

5. Discussion

A comparison between the severe and non-severe downbursts can help reveal which precursor signatures might prove most useful in predicting downburst severity. Both downbursts exhibited DRCs, rendering any method relying solely upon this precursor signature less able to distinguish between severe and non-severe downbursts. Subtle differences did exist between the DRCs, however. A lag between descent of the bottom and top of the high-reflectivity core was observed with the severe downburst, but was not clearly present with the non-severe downburst. The top of the core continued to descend between the time of initial downburst sampling and the time of maximum downburst intensity with the severe case. Conversely, the top of the core actually ascended slightly during this same time period with the non-severe downburst. Evolution and magnitude of the midlevel convergence did show noticeable differences between the two downbursts. The pattern of midlevel convergence with the severe downburst showed a marked increase to an extreme value before decreasing steadily. On the other hand, the convergence magnitude remained almost unchanged in the minutes leading up to the non-severe downburst’s occurrence. In addition, the maximum magnitude of convergence with Null-b never exceeded -.0003 s^{-1}, which is more than two times less than

that associated with MAB-a. The lack of strong convergence with the non-severe downburst matched expectations from the concept of mass continuity. Without the presence of strong descending motion in the 1–7 km layer, strong radial convergence was not sampled by weather radar. This difference in convergence magnitude is not likely due to differences in radar sampling since both downbursts occurred at approximately equal ranges and were moving in similar directions. These characteristics allowed the PAR to sample similar radial motion components for both downbursts. Due to the differences in the observed pattern and maximum magnitude, midlevel convergence appears to be a more robust indicator of downburst intensity.

6. Conclusion

The 14 June 2011 multicellular thunderstorm complex produced a unique opportunity to take advantage of the rapid-sampling capabilities of the PAR in observing a series of rapidly evolving downbursts. Continuous, rapid descent of the top of the high-reflectivity core occurred about eight minutes prior to each downburst's maximum intensity, while a short-lived peak in midlevel convergence occurred eight minutes prior to the severe downburst's maximum intensity and 11 minutes prior to the damaging wind report. In an operational setting, observations using the PAR support previous studies (e.g., Isaminger 1988; Roberts and Wilson 1989; Heinselman et al. 2008) that recommended using multiple precursor signatures to anticipate the occurrence of severe downbursts. In this case, a DRC may alert a forecaster to potential downburst development, while an increase in midlevel convergence magnitude could increase confidence that a severe downburst is more likely to occur. This result agrees with previous research that noted relationships between the magnitude of midlevel convergence and the strength of the surface divergence (Isaminger 1988). Dual-polarization precursor signatures may also prove beneficial in downburst warning operations, but an analysis of the utility of these signatures was not possible given the available temporal resolution and limited sample size. Data provided by a rapid-sampling observing system, such as a dual-polarization PAR, could aid in creating a more complete evolutionary picture of these precursor signatures and their operational implications.

Acknowledgements. We thank WDSS-II experts Karen Cooper, Kiel Ortega, and Robert Toomey; and software expert Eddie Forren for their extensive help during the course of this research.

REFERENCES

Balakrishnan, N. and D. S. Zrnić, 1990: Use of polarization to characterize precipitation and discriminate large hail. *J. Atmos. Sci.*, **47**, 1525–1540.

Brown, R. A., and V. T. Wood, 2000: Improved WSR-88D scanning strategies for convective storms. *Wea. Forecasting*, **15**, 208–220.

——, R. M. Steadham, B. A. Flickinger, R. R. Lee, D. Sirmans, and V. T. Wood, 2005: New WSR-88D volume coverage pattern 12: Results of field tests. *Wea. Forecasting*, **20**, 385–393.

Doviak, R. J., and D. S. Zrnić, 1993: *Doppler Radar and Weather Observations*. Academic Press, 562 pp.

Eilts, D. M., 1987: Nowcasting low-altitude wind shear with a Doppler radar. *AIAA 25th Aerospace Sciences Meeting*, Reno, NV, American Institute of Aeronautics and Astronautics, 1–5.

Fujita T. T., and H. R. Byers, 1977: Spearhead echo and downburst in the crash of an airliner. *Mon. Wea. Rev.*, **105**, 129–146.

——, 1981: Tornadoes and downbursts in the context of generalized planetary scales. *J. Atmos. Sci.*, **38**, 1511–1534.

——, and R. M. Wakimoto, 1981: Five scales of airflow with a series of downbursts on 16 July 1980. *Mon. Wea. Rev.*, **109**, 1438–1456.

Heinselman P. L., D. L. Priegnitz, K. L. Manross, T. M. Smith, and R. W. Adams, 2008: Rapid sampling of severe storms by the National Weather Radar Testbed Phased Array Radar. *Wea. Forecasting*, **23**, 808–824.

——, and S. M. Torres, 2011: High-temporal-resolution capabilities of the National Weather Radar Testbed Phased-Array Radar. *J. Appl. Meteor. and Climate*, **50**, 579–593.

Isaminger, A. M., 1988: A preliminary study of precursors to Huntsville microbursts. Lincoln Laboratory Project Report, 28 pp.

NWS Performance management, cited 2011. [Available online at https://verification.nws.noaa.gov.]

Proctor, F., H., 1988: Numerical simulations of an isolated microburst. Part I: Dynamics and Structure. *J. of Atmos. Sci.*, **45**, 3137–3160.

Roberts, R. D., and J. W. Wilson, 1989: A proposed microburst nowcasting procedure using single-Doppler Radar. *J. Appl. Meteor.*, **28**, 285–303.

Smith, T. M., and K. L. Elmore, 2004: The use of radial velocity derivatives to diagnose rotation and divergence. Preprints, *11th Conf. on Aviation, Range, and Aerospace*, Hyannis, MA, Amer. Meteor. Soc., CD-ROM, P5.6.

Srivastava, R.C, 1985: A simple model of evaporatively driven downdraft: Application to microburst downdraft. *J. of Atmos. Sci.*, **42**, 1004–1023.

——, 1987: A model of intense downdrafts by the melting and evaporation of precipitation. *J. Atmos. Sci.*, **44**, 1752–1773.

Straka, J. M., and J. R. Anderson, 1993: Numerical simulations of microburst-producing storms: Some results from storms observed during COHMEX. *J. Atmos. Sci.*, **50**, 1329–1348.

Vasiloff, S. V., and K. W. Howard, 2009: Investigation of a severe downburst storm near Phoenix, Arizona, as seen by a mobile Doppler radar and the KIWA WSR-88D. *Wea. Forecasting*, **24**, 856–867.

Wakimoto, R. M., and V. N. Bringi, 1988: Dual-polarization observations of microbursts associated with intense convection: The 20 July storm during the MIST project. *Mon. Wea. Rev.*, **116**, 1521–1539.

Zrnić, D. S., and A. V. Ryzhkov, 1999: Polarimetry for weather surveillance radars. *Bull. Amer. Meteor. Soc.*, **80**, 389–406.

——, 2001: Convectively driven high wind events. *Severe Convective Storms, Meteor. Monogr.*, No. 50. Amer. Meteor. Soc., 255–298.

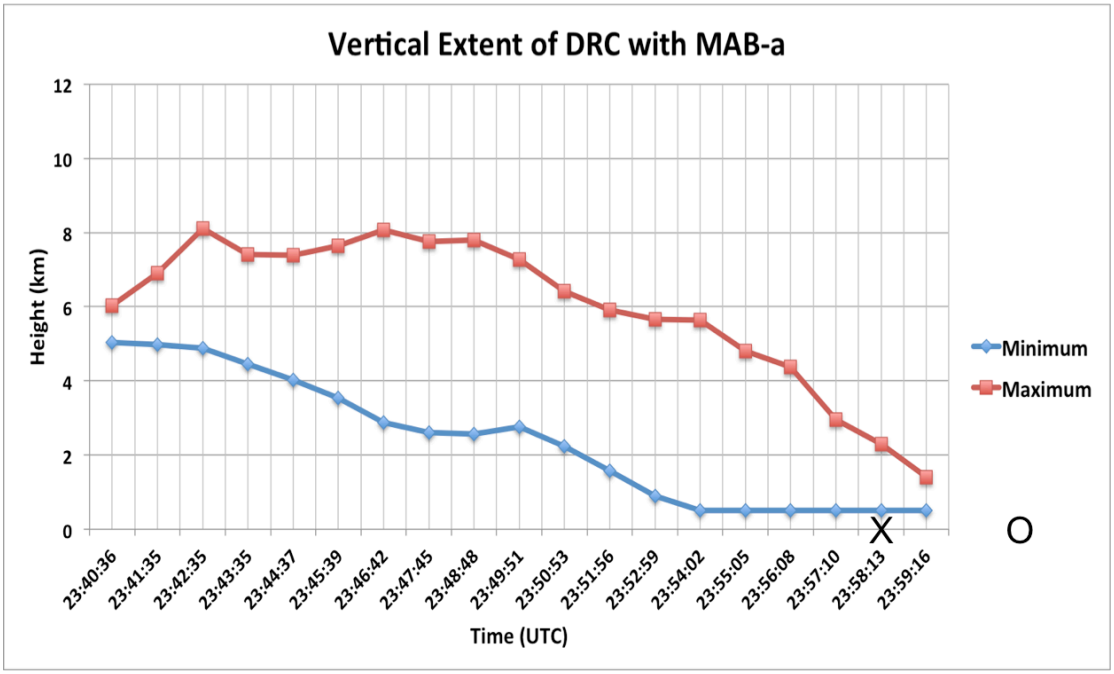

Figure 3. Evolution of the 65 dBZ isosurface associated with the severe downburst. The red line shows the maximum height (MSL) of the 65 dBZ isosurface, while the blue line shows the minimum height. X marks the initial sampling time of the near surface divergent signature, while the O marks the sampling time of the maximum base velocity (0002 UTC).

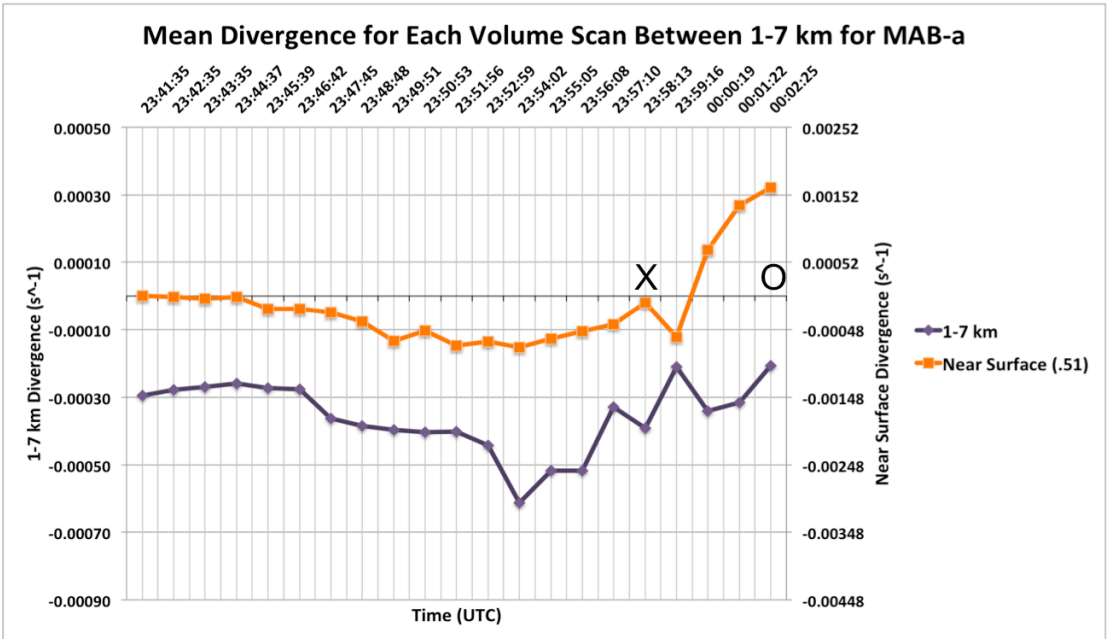

Figure 4. Evolutionary pattern and magnitude of the mean 1-7 km divergence associated with the severe downburst. Negative values correspond to radial convergence, while positive values correspond to radial divergence. The dark purple line shows the magnitude of the mean 1-7 km divergence, and the orange line shows the magnitude of the near surface divergence. X marks the initial sampling time of the near surface divergent signature, while the O marks the sampling time of the maximum base velocity.

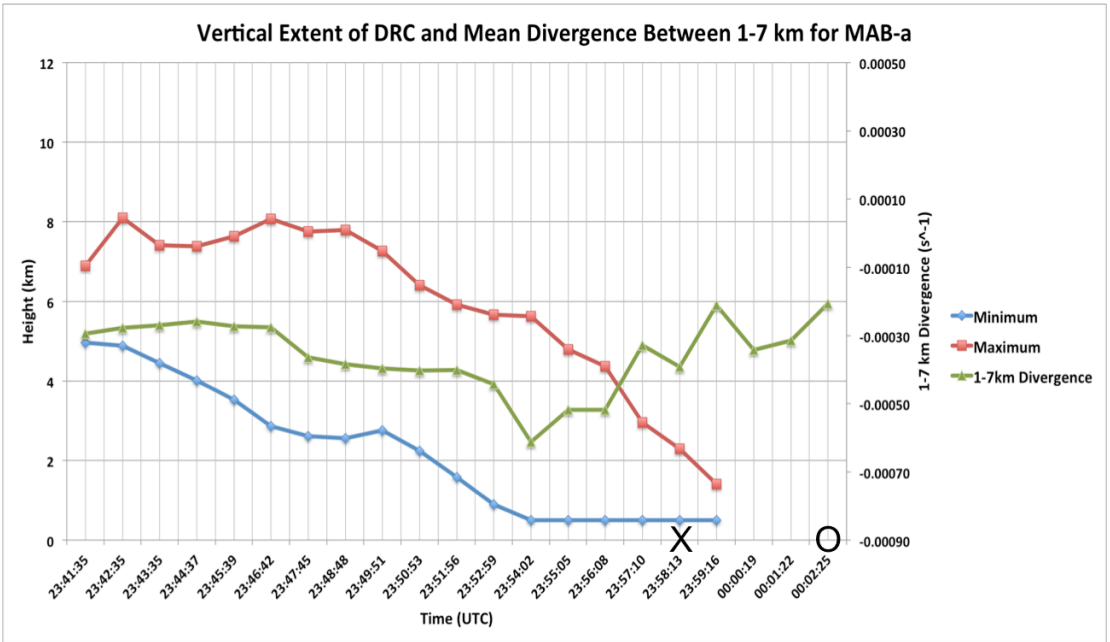

Figure 5. Evolution of the 65 dBZ isosurface and the 1-7 km mean divergence with the severe downburst. The red line shows the maximum height (MSL) of the 65 dBZ isosurface, while the blue line shows the minimum height. Mean 1-7 km divergence is shown in green. X marks the initial sampling time of the near surface divergent signature, while the O marks the sampling time of the maximum base velocity.

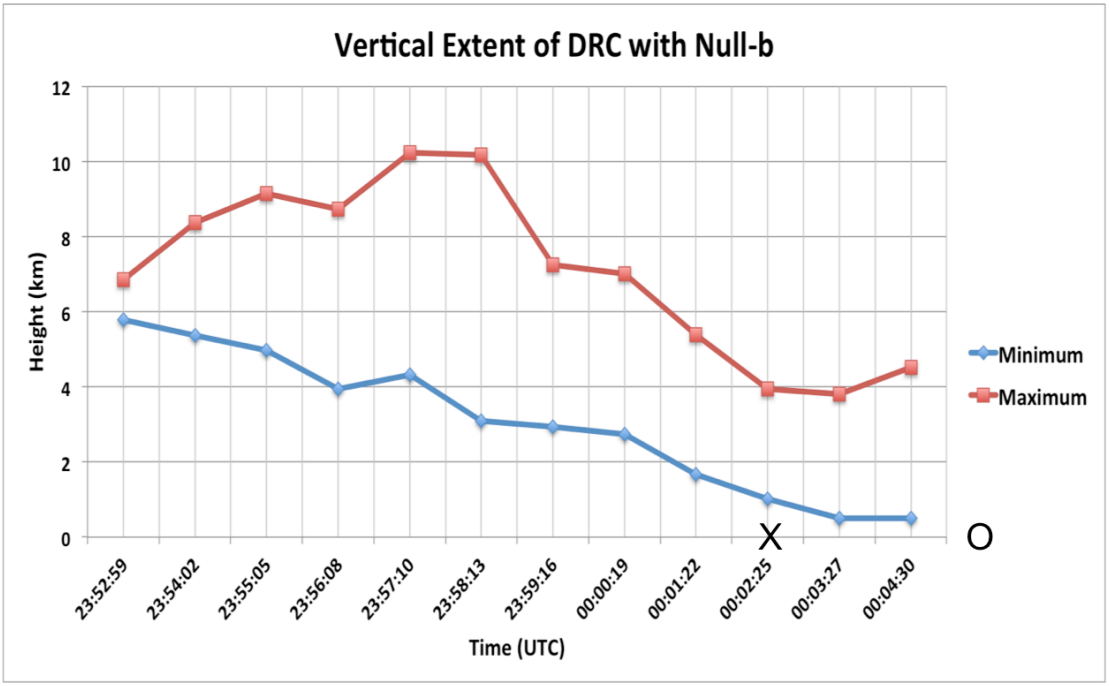

Figure 6. Evolution of the 65 dBZ isosurface associated with the non-severe downburst. The red line shows the maximum height (MSL) of the 65 dBZ isosurface, while the blue line shows the minimum height. X marks the initial sampling time of the near surface divergent signature, while the O marks the sampling time of the maximum base velocity (0006 UTC).

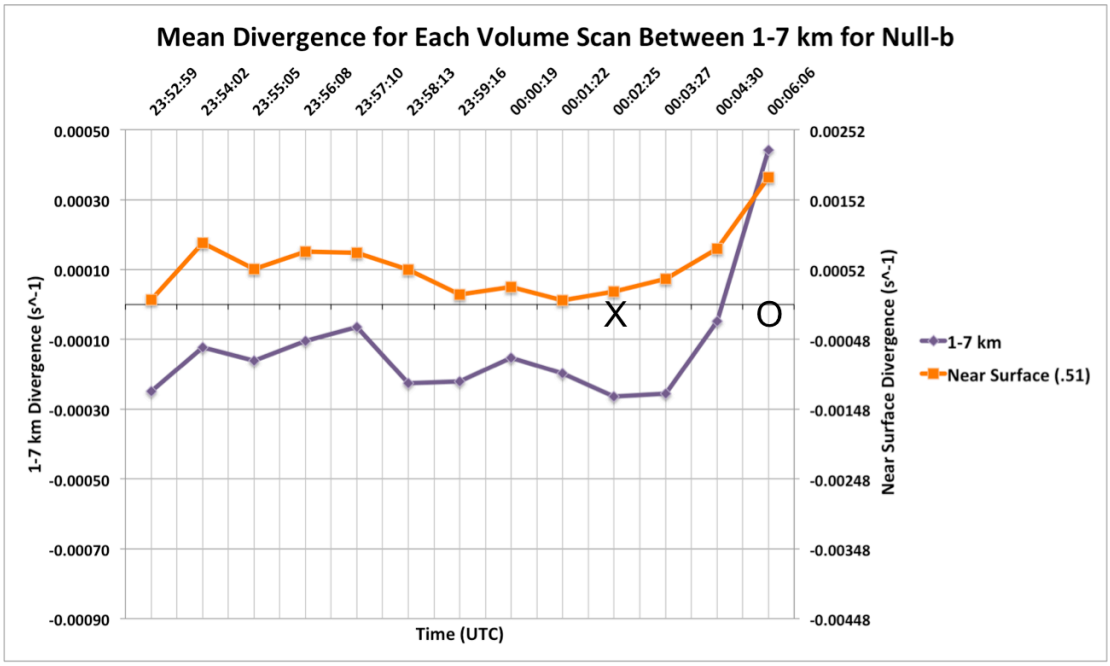

Figure 7. Evolutionary pattern and magnitude of the 1-7 km mean divergence associated with the non-severe downburst. Negative values correspond to radial convergence, while positive values correspond to radial divergence. The dark purple line shows the magnitude of the mean 1-7 km divergence, and the orange line shows the magnitude of the near surface divergence. X marks the initial sampling time of the near surface divergent signature, while the O marks the sampling time of the maximum base velocity.